# Spatiotemporal diffusion as early warning signal for critical transitions in spatial tumor-immune system with stochasticity

Zhiqin Ma,[1] Yuhui Luo,[1] Chunhua Zeng,[1,2,*] and Bo Zheng[3,2]

[1]*Faculty of Science, Kunming University of Science and Technology, Kunming 650500, China*
[2]*Department of Physics, Zhejiang University, Hangzhou 310027, People's Republic of China*
[3]*School of Physics and Astronomy, Yunnan University, Kunming 650091, People's Republic of China*

(Received 19 July 2021; accepted 22 March 2022; published 14 April 2022)

Complex dynamical systems have tipping points and exhibit nonlinear dynamics. It is difficult to predict and prevent the onset and progression of the tumors, mainly due to the complexity of interactions between tumor growth and tumor-immune cells involved. Moreover, previous models were based on the influence of the zero-dimensional systems and did not consider the spatiotemporal fluctuation in the tumor microenvironment. We here extend the previous model to a two-dimensional system and employ spatial early warning signals to study the spatially extended tumor-immune system with stochasticity. On the one hand, we obtain the stationary probability density of the system under the mean-field approximation assumption. It is found that the health state gets more and more stable than the disease state as the noise level increases when the system has a bistable state, and the system goes from health to disease state through a bistable region as the growth rate increases. On the other hand, we present a spatiotemporal diffusion coefficient indicator to predict upcoming critical transitions. It is shown that a rising spatiotemporal diffusion coefficient obtained from the spatial snapshot data can be an effective indicator for predicting upcoming critical transitions. Anticipating critical transitions in the spatial tumor-immune system with stochasticity can be greatly helpful to prevent disease onset and progression, which may intercept abrupt shifts from health to disease state.

DOI: 10.1103/PhysRevResearch.4.023039

## I. INTRODUCTION

Some ecosystems and biological systems are complex, characterized by abrupt shifts, and usually comply with nonlinear dynamics [1]. Moreover, many complex systems have tipping points where their equilibrium state abruptly shifts from one stable state to another [2]. These shifts are referred to as regime shifts or critical transitions [3]. In the past decade, several studies provided evidence for the presence of critical transitions in ecosystems. In ecology [4], critical transitions have been related to the eutrophication of lakes [5–7], the collapse of fish populations [8], algae overgrowth coral reefs [9,10], and Dansgaard-Oeschger events in Greenland [11]. There are similar characteristics in biological systems and ecosystems, i.e., critical transitions. In biology, already identified critical transitions have also been associated with microbiome dysregulation [12], depression [13], epileptic seizures [14,15], and cancer [16]. Theoretical and empirical studies indicate that the notion of critical transitions and tipping points has been applied to biological systems [1].

The evolution of spatial patterns has been an important concept and extensively studied in biophysical and biochemical systems [17–21]. Their classification systems include the Ginzburg-Landau model [22], the Swift-Hohenberg equation [23,24], the Belousov-Zhabotinsky reaction [25,26], and the Synchronization [27,28]. In particular, there is evidence that spatial patterns play a crucial role in the growth and development of tumors. Examples include solid tumor growth models [29,30], avascular tumor growth models [31,32], invasive tumor growth coupled reaction-diffusion equations [33], and stratified epithelia nutrient-diffusion dynamics [34]. The majority of previous studies on the modeling of the tumor microenvironment (TME) are based on spatial pattern formation. A majority of these studies have mostly ignored quantitative research of tumor cell populations. Moreover, in previous studies, these systems only involved the time dimension and were not sufficient to describe the real environment of tumor growth [35–37]. To simplify the analysis, our model simplifies the parametrization of the TME, namely, the model assumes a constant reserve of immune cells that serve to kill tumor cells. A simplified model of tumor growth and tumor-immune cell interactions can allow for focusing on two aspects: (1) Studying the influence of a stochastic growth rate and a diffusion of the tumor cells in the overall competition and (2) developing spatial warning signals for critical transitions between low and high tumor density states. Furthermore, in spatially extended tumor-immune systems with stochasticity, the local dynamics are coupled between neighboring sites, a characteristic that is obviously inexistent in purely temporal systems

*chzeng83@kust.edu.cn; zchh2009@126.com

[38]. It is worth noting that stochasticity has also been the subject of classic studies in nonlinear dynamics [38,39]. In this paper, we extend the previous system to the spatially extended tumor-immune system with stochasticity to study how spatiotemporal noise (stochastic growth rate) and diffusion (connectivity) affect the behavior of the system.

It is difficult to predict these critical transitions as the equilibrium state of the system may display little change until the tipping point is reached [2]. In addition, it is impossible to thoroughly study the mechanisms and parametrizations of the various complex systems [40]. Although it is extremely difficult to predict critical transitions before they are reached, work in different scientific fields has shown the existence of generic early warning signals [41]. These early warning signals have been applied to complex systems, such as ecosystems [4,21,42,43], climate [11,44], biological systems [45,46], and financial markets [47,48]. One issue is that the detection of critical transitions from time series inclines to require long, high-resolution data [49]. In other words, time series might offer insufficient information to find upcoming critical transitions. Then will spatial indicators accurately reveal early warning signals more than time indicators? Because a spatial snapshot can carry much more information than a single point in a time series, spatial indicators are a potentially forceful option [49]. Here we aim to provide spatial early warning signals (SEWSs) of critical transition in the spatially extended tumor-immune systems with stochasticity.

The paper is organized as follows. In Sec. II A, we present the dynamical model of the spatially extended tumor-immune system with stochasticity [37]. In Sec. II B, through the mean-field approximation (MFA) assumption, we derive a corresponding Fokker-Planck equation from the Langevin equation and give the stationary probability distribution solution. In Sec. II C, we propose the metric-based spatial indicators to predict upcoming critical transitions. In Sec. III A, we study the effect of the noise levels $Q$ and growth rates $r$ in the spatially extended tumor-immune system with stochasticity by calculating the stationary probability distributions. In Sec. III B, we present a novel indicator to identify upcoming critical transitions in the spatially extended tumor-immune systems with stochasticity. In Sec. IV, we briefly summarize the results for the spatial tumor-immune system with stochasticity.

## II. MODEL AND METHODS

### A. Model description

The tumor growth under immune surveillance can be described by the insect outbreak model [50,51]. We simplify the problem by exploiting a separation of time scales: the tumor cell population evolves on a fast time scale (their doubling time is generally several months, so they have a characteristic time scale of months), whereas the nutrients are stored on a slow time scale (at a much slower rate than tumor cells, they consume their stored nutrients in the case of tumor cell density above a critical threshold, and the human life span in the absence of cancer is between 70 and 100 years so that their generation time is measured in decades) [50]. Thus the minimum number of variables will include tumor cell population as a fast variable and nutrient storage quantity as a slow variable. It means that in this case, nutrient storage variables may be treated as constants. In addition, the main limiting features for tumor growth are nutrient supply and the effects of immune cells. Therefore the model for the tumor growth and tumor-immune cell interactions can be written as [52,53]

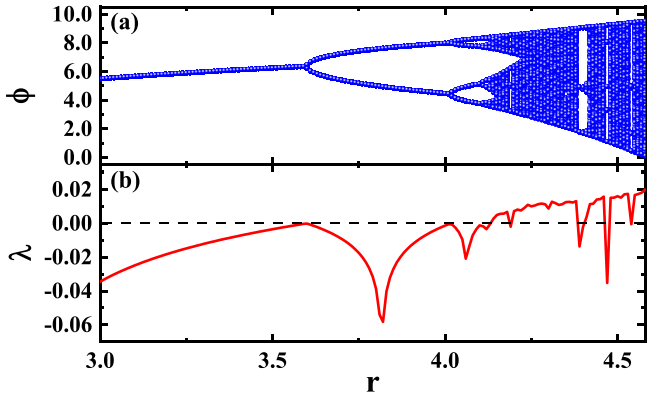


FIG. 1. (a) The bifurcation diagram and (b) Lyapunov exponent as a function of $r$, respectively. The parameters are chosen as $\beta = 2.0$ and $K = 10.0$.

$$\frac{d\hat{\phi}}{d\hat{t}} = \hat{r}\hat{\phi}\left(1 - \frac{\hat{\phi}}{\hat{K}}\right) - p(\hat{\phi}), \tag{1}$$

where $\hat{\phi}$ denotes the tumor nuclei density, $\hat{r}$ represents growth rate, and the carrying capacity $\hat{K}$ is assumed to depend on the nutrients available. $p(\hat{\phi}) = \beta\hat{\phi}^2/(\epsilon^2 + \hat{\phi}^2)$ represents the immune term with the ability to recognize and eliminate nascent tumors [51]. Here $\beta$ is the immune coefficient, and $\epsilon$ is the critical level. The physical significance of the immune term suggests that immune cells increase with increasing tumor cells. However, once the tumor cell density exceeds a certain critical level $\phi = \epsilon$, the immune system turns on sharply and then saturates (the immune cells are working as fast as they can). The dimensionless form [54,55] of Eq. (1) is given by

$$\frac{d\phi}{dt} = r\phi\left(1 - \frac{\phi}{K}\right) - \frac{\beta\phi^2}{1+\phi^2}, \tag{2}$$

where $\phi = \hat{\phi}/\epsilon$, $t = \hat{t}/\epsilon$, $r = \hat{r}\epsilon$, and $K = \hat{K}/\epsilon$. Here $r$, $K$, and $\beta$ are the dimensionless growth rate, carrying capacity, and immune coefficient, respectively.

It should be noted that the early work had discussed the discrete tumor growth model [56] in pathology of which a detailed description is given in Appendix A. As shown in Fig. 1, the bifurcation diagram reveals the appearance of the transition from order to the chaotic system with increasing growth rate $r$. The TME mainly includes tumor cells, immune cells, and stromal cells [57]. The interaction of two or more subpopulations of cancer cells may lead to negative, neutral, and positive selection for tumor evolution [57]. It is worth mentioning that the TME has a strong influence on cancer evolution [57], which suggests the existence of spatiotemporal fluctuations [58,59] in growth rate $r$. Therefore the growth rate $r$ in Eq. (2) should be rewritten as $r + \eta(\mathbf{x}, t)$. Here $\eta(\mathbf{x}, t)$ is a Gaussian white noise in both time and space with zero mean

and the correlation function is given by

$$\langle \eta(\mathbf{x},t)\eta(\mathbf{x}',t')\rangle = 2Q\delta(\mathbf{x}-\mathbf{x}')\delta(t-t'), \tag{3}$$

where $Q$ is the noise level. Connectivity is modeled as the exchange of tumor nuclei density between neighboring lattices mimicked through a simple diffusive process. As such, the stochastic partial differential equation (SPDE) in the most standard form [40,59] can be written as

$$\frac{\partial\phi(\mathbf{x},t)}{\partial t} = r\phi\left(1-\frac{\phi}{K}\right) - \frac{\beta\phi^2}{1+\phi^2} + D\nabla^2\phi + \phi\left(1-\frac{\phi}{K}\right)\eta(\mathbf{x},t), \tag{4}$$

where $\phi(\mathbf{x},t)$ is density variable in the spatial lacation $\mathbf{x}$ at time $t$ and $D$ denotes diffusion coefficient.

To simplify the simulation, we consider a lattice form in $d$ dimension. Each lattice is connected with its four neighboring lattices. Partition space (see Appendix B) into $N = L^d$ squares of lattice spacing $\Delta x$, Eq. (4), can be rewritten as [38,39,60]

$$\frac{\mathrm{d}\phi_i(t)}{\mathrm{d}t} = r\phi_i\left(1-\frac{\phi_i}{K}\right) - \frac{\beta\phi_i^2}{1+\phi_i^2} + \frac{D}{2d\Delta x^d}\sum_{j\in nn(i)}(\phi_j-\phi_i) + \phi_i\left(1-\frac{\phi_i}{K}\right)\eta_i(t), \tag{5}$$

where $nn(i)$ represents the set of $2d$ nearest neighbors of site $i$ and $d$ denotes space dimension. For the white noise, the correlation function of Eq. (3) can be rewritten as

$$\langle \eta_i(t)\eta_j(t')\rangle = 2\frac{Q}{\Delta x^d}\delta_{ij}\delta(t-t'). \tag{6}$$

### B. Theoretical analysis

The MFA is achieved through the following assumptions [38]:

$$\frac{D}{2d\Delta x^d}\sum_{j\in nn(i)}(\phi_j-\phi_i) = \frac{D}{\Delta x^d}(\langle\phi\rangle-\phi_i). \tag{7}$$

Let $f[\phi_i(t)] = r\phi_i(t)[1-\phi_i(t)/K] - \beta\phi_i^2(t)/[1+\phi_i^2(t)]$ and $g[\phi_i(t)] = \phi_i(t)[1-\phi_i(t)/K]$; one can obtain the corresponding Fokker-Planck equation of Eq. (5) under the MFA assumption Eq. (7) written in the Stratonovich interpretation ($\alpha = 1/2$) as [61–63]

$$\frac{\partial P(\{\phi_i\},t)}{\partial t} = -\frac{\partial[A(\{\phi_i\})P(\{\phi_i\},t)]}{\partial\{\phi_i\}} + \frac{\partial^2[B(\{\phi_i\})P(\{\phi_i\},t)]}{\partial\{\phi_i\}^2}, \tag{8}$$

where

$$A(\{\phi_i\}) = f(\{\phi_i\}) + \frac{D}{\Delta x^d}(\langle\phi\rangle-\{\phi_i\}) + Qg(\{\phi_i\})g'(\{\phi_i\}),$$
$$B(\{\phi_i\}) = Q[g(\{\phi_i\})]^2. \tag{9}$$

For convenience, we drop the subscript $i$. Evaluation of the quantity $\langle\phi\rangle$ is introduced, which is the solution of MFA, and then it can be written as [38]

$$\langle\phi\rangle = F(\langle\phi\rangle) = \int \phi P_{st}(\phi,\langle\phi\rangle)\,d\phi. \tag{10}$$

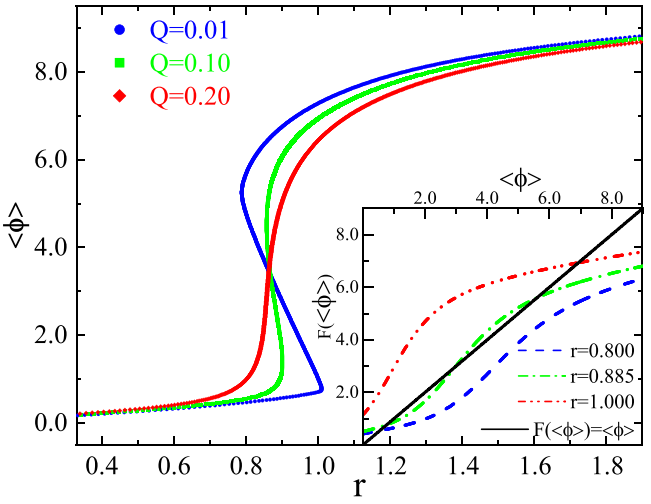


FIG. 2. The MFA of solutions $\langle\phi\rangle$ as a function of growth rate $r$ for three different noise intensities $Q$. These points correspond to the intersection of these curves in the inset. Inset: The set of solutions, $\langle\phi\rangle$, of the self-consistency equation (10) is the intersection point between $F(\langle\phi\rangle) = \langle\phi\rangle$ and $F(\langle\phi\rangle) = \int \phi P_{st}(\phi,\langle\phi\rangle)\,d\phi$ for noise level $Q = 0.01$ (data not shown), $Q = 0.10$, and $Q = 0.20$ (data not shown). Other parameter values are $\beta = 2.0$, $K = 10.0$, and $D = 0.1$.

Equation (10) is a self-consistency equation because the stationary probability distribution relies on unknown variables $\langle\phi\rangle$. Consequently, finding the set of solutions of this self-consistency equation is solving the MFA.

We use the secant intersection method to solve the transcendental equation of Eq. (10) [60]. Figure 2 shows that through the intersection point between $F(\langle\phi\rangle) = \langle\phi\rangle$ and $F(\langle\phi\rangle) = \int \phi P_{st}(\phi,\langle\phi\rangle)\,d\phi$, we can obtain the solution $\langle\phi\rangle$ as a function of growth rate $r$. It is clear that the solutions of the self-consistency equation exhibit a monostable state for the low and high values of $r$ and bistable states for a range of intermediate values of $r$. Namely, the increase of noise leads to the transition from three equilibria to an equilibrium of the solution of the self-consistency equation. This finding suggests that the noises play a significant role in the critical transitions.

The corresponding stationary probability distribution solution $P_{st}(\phi,\langle\phi\rangle)$ of Eq. (8) reads [64,65]

$$\begin{aligned} P_{st}(\phi,\langle\phi\rangle) &= \frac{N}{B(\phi)}\exp\int^{\phi}\frac{A(\phi')}{B(\phi')}\,d\phi' \\ &= \frac{N}{\sqrt{Q}g(\phi)}\exp\int^{\phi}\frac{f(\phi')}{B(\phi')}\,d\phi' \\ &= N\exp\left[\int^{\phi}\frac{f(\phi')}{B(\phi')}\,d\phi' - \ln\sqrt{Q}g(\phi)\right] \\ &= N\exp\left[-\frac{U_{\mathrm{eff}}(\phi,\langle\phi\rangle)}{Q}\right], \end{aligned} \tag{11}$$

where $N$ is the normalization constant. $U_{\mathrm{eff}}(\phi,\langle\phi\rangle)$ is the effective potential (landscape) and it can be expressed as

follows:

$$U_{\text{eff}}(\phi, \langle\phi\rangle) = \frac{2\beta K^3}{(1+K^2)^2}\left(\ln\left|\frac{K\sqrt{1+\phi^2}}{K-\phi}\right| + \frac{K}{2}\arctan\phi\right) + (r+Q-D)\ln\left|\frac{K-\phi}{\phi}\right| + \frac{\beta K^2}{(1+K^2)^2}\left(\frac{1}{K-\phi} - \arctan\phi + \frac{K^2}{K-\phi}\right) + Q\ln\left|\frac{\sqrt{Q}\phi^2}{K}\right| + \frac{DK}{K-\phi} + \frac{D\langle\phi\rangle K - 2\phi}{\phi(K-\phi)} + \frac{2D\langle\phi\rangle}{K}\ln\left|\frac{K-\phi}{K\phi}\right|. \quad (12)$$

### C. Metric-based spatial indicators

In this work, metric-based spatial indicators quantify alternations in the statistical properties of the spatial datasets produced by Eq. (5). Moreover, they can be used to identify impending critical transitions between alternative stable states in complex systems. These indicators have been fully verified in complex systems, such as ecosystems [4,21], climate [11,44], biological systems [45,46], and financial markets [47,48].

#### 1. Spatial variance

Critical slowing down can give rise to larger fluctuations near the equilibrium state of the system, which leads to the increase of spatial variance of the system before a transition. Here we define the spatial variance functions of the state variable as [6,40]

$$\sigma^2 = \frac{1}{N}\sum_{i=1}^{N}(\phi_i - \bar{\phi})^2, \quad (13)$$

where $N$ is the total number of spatial units. $\phi_i$ denotes the attribute value of the spatial unit $i$, and the subscript $i$ stands for $d$-dimension space; $\bar{\phi}$ is the average of all spatial unit values.

#### 2. Spatial skewness

When the system approaches a transition, spatial patterns can become increasingly asymmetric. The spatial asymmetry can be measured by spatial skewness, which is defined by [21,40]

$$\gamma = \frac{1}{N\sigma^3}\sum_{i=1}^{N}(\phi_i - \bar{\phi})^3. \quad (14)$$

#### 3. Spatial kurtosis

Fluctuations can cause the spatial kurtosis of states of a system to reach more extreme values close to a transition. This kurtosis is the standardized fourth moment of fluctuations of state variable and is defined by [66]

$$\kappa = \frac{1}{N\sigma^4}\sum_{i=1}^{N}(\phi_i - \bar{\phi})^4. \quad (15)$$

#### 4. Near-neighbor spatial correlation

The near-neighbor spatial correlation [20,67,68] (at lag-1) captures the increasing correlation among neighboring spatial sites. It can be quantified by the spatial correlation function between biological states $\phi_i$ and $\phi_j$ separated by a distance $R$; thus it is defined by

$$\mathbb{C}(R) = \frac{N\sum_{i=1}^{N}\sum_{j=1}^{N}\omega_{ij}(\phi_i - \bar{\phi})(\phi_j - \bar{\phi})}{W\sum_{i=1}^{N}(\phi_i - \bar{\phi})^2}, \quad (16)$$

where $W = \sum_{i=1}^{N}\sum_{j=1}^{N}\omega_{ij}$ is the total number of units separated by distance $R$; $\omega_{ij}$ is the spatial weight matrix. It is equal to 1 if spatial units $i$ and $j$ are separated by a distance $R$ and to 0 otherwise; $\phi_i$ and $\phi_j$ represent the attribute value of the spatial unit $i$ and the spatial unit $j$, respectively.

#### 5. Near-neighbor spatiotemporal diffusion coefficient at lag-1

The spatiotemporal dispersion at time lag $\tau$ and neighboring units separated by the distance $R$ are given by

$$\delta\phi_{ij}(t) = \omega_{ij}[\phi_j(t) - \phi_i(t-\tau)]. \quad (17)$$

The spatiotemporal diffusion coefficient is characterized by the mean-square deviation of the density variable $\delta\phi_{ij}(t)$ in the spatial locations $i$ and $j$ at time $t$ [69–72], namely,

$$\mathbb{D}(R,\tau) = \frac{1}{N^2}\sum_{i=1}^{N}\sum_{j=1}^{N}\frac{\langle\delta\phi_{ij}^2(t)\rangle - \langle\delta\phi_{ij}(t)\rangle^2}{4\tau}. \quad (18)$$

In our numerical simulation, both $R$ and $\tau$ are taken as 1, thus $\mathbb{C}(R) = \mathbb{C}(1)$ and $\mathbb{D}(R,\tau) = \mathbb{D}(1,1)$.

## III. RESULTS

### A. Stationary probability distribution function

To validate the theoretical results obtained from the stationary probability density function (SPDF) of Eq. (11), we employ the stochastic Heun algorithm [59,73] to simulate stochastic dynamics. The derivation of this algorithm is given in Appendix B. To obtain convergent results, we run the simulations for $10^7$ time steps and remove $10^6$ initial transient state data. The numerical simulations of Eqs. (5) and (6) are performed on a square lattice of $128 \times 128$ cells of grid size $\Delta x = 1$ with a time step $\Delta t = 0.001$ and periodic boundary conditions. The initial conditions of $\phi_i(0)$ were uniformly distributed over the interval [0,1].

The theoretical results and the numerical simulations of the SPDF are plotted in Figs. 3(a)–3(c) for different noise levels $Q$. When the noise level is small, the numerical simulations (symbols) agree well with the theoretical prediction (solid lines), suggesting that our results are credible. For the monostable region, the SPDF peaks decrease with the increases of the noise level $Q$, as shown in Figs. 3(a) and 3(c). For the bistable region, however, with the increase of the noise level $Q$, the SPDF peak increases at low tumor nuclei density

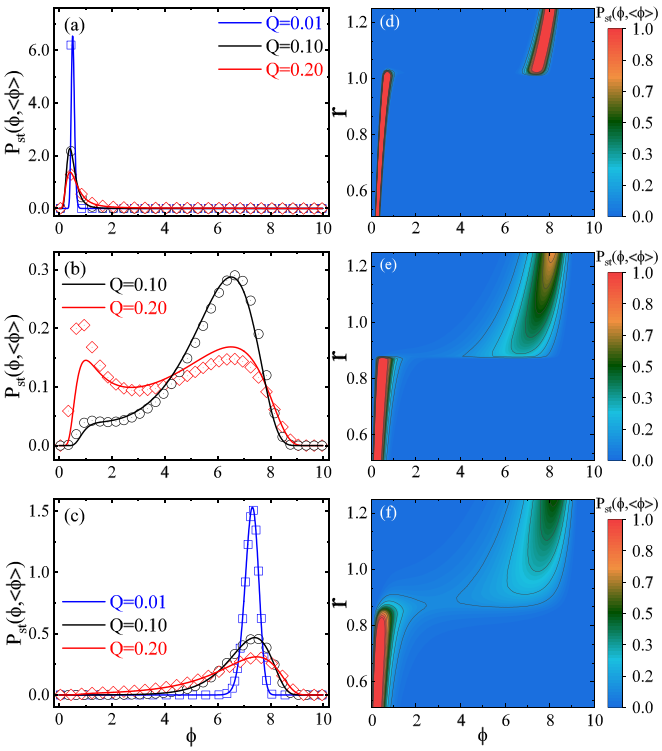


FIG. 3. [(a)–(c)] The stationary probability distribution function $P_{st}(\phi, \langle\phi\rangle)$ for different noise levels $Q$ and growth rates $r$: (a) $r = 0.800$, (b) $r = 0.885$, and (c) $r = 1.000$. The symbols represent simulation results, and the solid lines depict the theoretical results of Eq. (11). [(d)–(f)] The contour plot of numerical $P_{st}(\phi, \langle\phi\rangle)$ as a function of $\phi$ and $r$ for different noise levels $Q$: (d) $Q = 0.01$, (e) $Q = 0.10$, and (f) $Q = 0.20$. Other parameter values are the same as in Fig. 2.

state (health) and decreases at high tumor nuclei density state (disease), as shown in Fig. 3(b). These results indicate that when the system has a bistable state, the low tumor nuclei density state (health) gets more and more stable than the high tumor nuclei density state (disease) as the noise level increases. It should be noted that for $Q = 0.01$ and $r = 0.885$, the SPDF does not show a bistable state. This finding means that noise plays a key role in the existence of the bistable region. Moreover, for $r = 0.800$ (less than the critical value), the distribution shows a maximum for $\phi \approx 0.5$ [see Fig. 3(a)]. For $r = 0.885$ (close to the critical value), $P_{st}(\phi, \langle\phi\rangle)$ shows that the system can be found in either two states, one for $\phi \approx 1.0$, which corresponds to health state, and the other for $\phi \approx 7.0$, which corresponds to disease state [see Fig. 3(b)]. For $r = 1.000$ (greater than the critical value), the SPDF shows a single maximum for $\phi \approx 7.0$ [see Fig. 3(c)]. These results indicate that a bistable state will only occur in the critical region. Figures 3(d)–3(f) show the contour plot of $P_{st}(\phi, \langle\phi\rangle)$ in the $\phi - r$ plane. The figures show twofold results: on the one hand, when we increase the parameter $r$, the system undergoes from low tumor nuclei density (health) state to high tumor nuclei density (disease) state through a bistable region. On the other hand, as the noise increases, the bistable region will gradually become larger. These transitions of the SPDF from health to disease state are consistent with Zhong *et al.*, conforming to previous investigations [60].

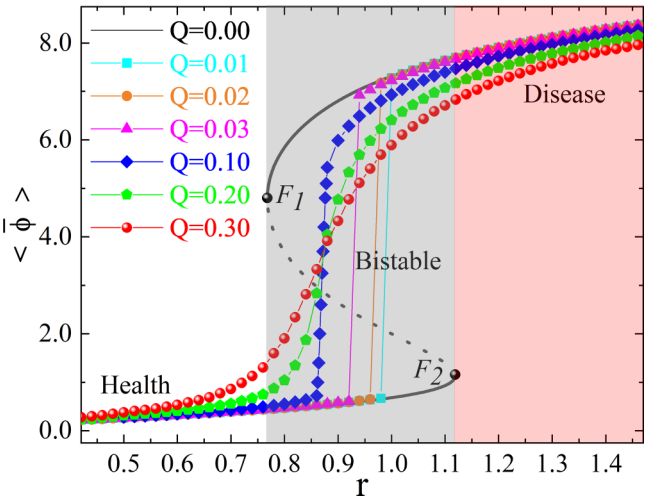


FIG. 4. The steady-state ensemble average of tumor nuclei density as a function of growth rate $r$ for different noise levels $Q$. The black curved lines denote stable (solid) and unstable (dashed) equilibria states. The black dots (saddle-node) are tipping points. Other parameter values are $\beta = 2.0$, $K = 10.0$, and $D = 0.1$.

The effect of simultaneously changing the growth rates $r$ together with the different noise levels $Q$ on the steady-state ensemble average is also depicted in Fig. 4. For the deterministic system of Eq. (2), the tipping points are $F_1$ and $F_2$, which divide the states of systems into three states: health state (white shaded region), bistable state (gray shaded region), and disease state (red shaded region). The black curved lines represent stable (solid) and unstable (dashed) equilibria; the black dots ($F_1$ or $F_2$) indicate tipping points. The dashed line in the middle of the bifurcation point represents the border between the basins of attraction of the two alternative stable states on the upper and lower branches. In Fig. 4, we observe that the effect of the noise level $Q$ is a displacement of the critical point toward lower values of growth rate $r$. These findings suggest that the noise induces earlier critical transitions. We also identify a critical growth rate $r$ that separates the health to the disease state of the system.

### B. SEWSs

To identify the transitions from a health state to a disease state, we use a recently developed toolbox for SEWSs [74] to anticipate critical transitions in the spatial tumor-immune system with stochasticity [21]. We assess the SEWSs of upcoming transitions by analyzing numerically simulated spatial datasets from Eq. (5). The numerical simulations are performed using the stochastic Heun algorithm (see Appendix B) with a time step $\Delta t = 0.001$ and periodic boundary conditions. All simulations are also started via the random introduction of tumor density states uniformly distributed over the interval [0,1]. We then increase the growth rate $r$ linearly in 10,000 time intervals from 0.6 to 1.6. After each stepwise alteration in the growth rate $r$, we run 1000 time steps to reduce transient effects [20]. At the finish of the 1000 time steps, we used the last obtained snapshot of the state variables to calculate the statistical properties of the spatial datasets. These properties can quantify the SEWSs, which antecede some disease state transitions.

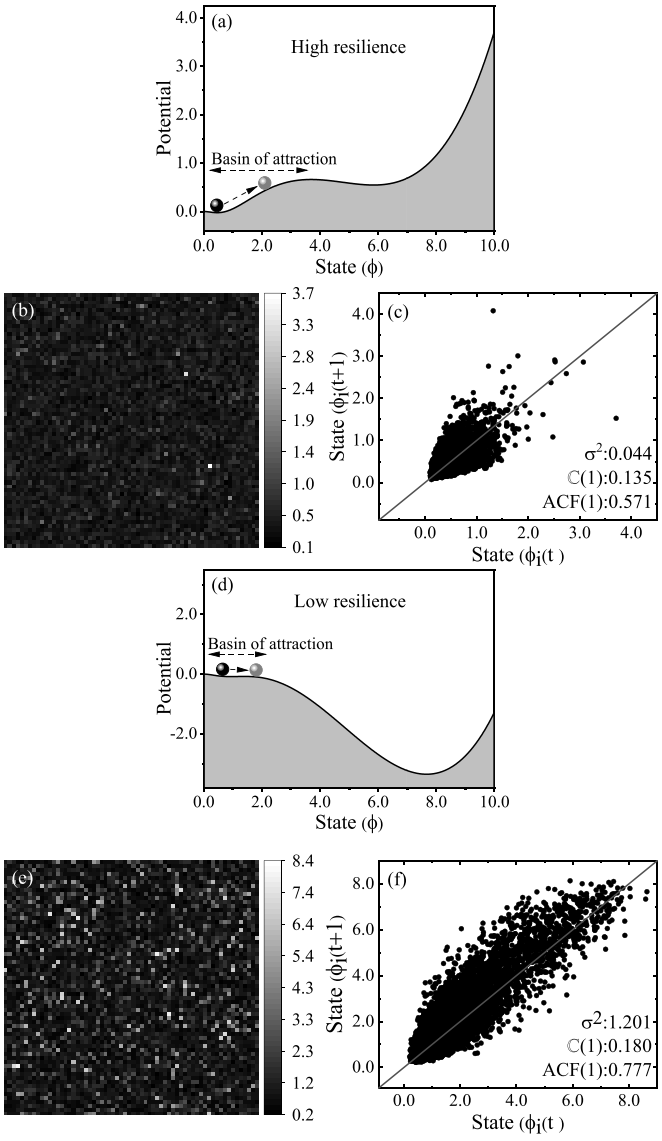


FIG. 5. CSD is an indicator in which the system has lost resilience. [(a)–(c)], Far from the transition point, resilience is large (a). [(d)–(f)], Close to the transition point, resilience is small (d). If the basin of attraction is small (d), the recovery rates on tiny perturbations are slower than when the basin of attraction is large (a). The effect of this reduced resilience may be measured in spatial snapshots in the state of the system [(b) and (e)] as increased spatial variance, the temporal autocorrelation function at lag-1 [ACF(1)], and the near-neighbor spatial correlation [(c) and (f)]. The parameter values are $\beta = 2.0$, $K = 10.0$, $D = 0.1$, $Q = 0.1$, and either $r = 0.8$ [(a)–(c)] or $r = 1.1$ [(d)–(f)].

To see SEWSs of the transition from health to disease state, we first investigate the phenomenon of critical slowing down (CSD) that the recovering rates of the system become increasingly slow from small perturbations. Namely, the system loses its resilience. Figures 5(a) and 5(d) show the stable landscapes far from and close to critical points of $r$. The slopes of the this landscape and the size of the basin of attraction around equilibrium can be related to its resilience that is defined as the ability of the system to recover from small disturbances. This resilience is expressed not only in spatial snapshots but also in time characteristics [75]. These results reveal that as the system approaches critical points, certain characteristics change in the spatial snapshots [see Figs. 5(b) and 5(e)] and the short-term memory of time data are expected to occur. One important prediction is that the CSD should lead to an increase in spatial variance in near-neighbor spatial correlation and in temporal autocorrelation function at lag-1 [66] [see Figs. 5(c) and 5(f)]. Hence the CSD has also been considered as an indicator of whether a system is approaching a critical transition.

The spatial datasets obtained by Eq. (5) are used to calculate the transient-state ensemble average and the following warning indicators: Near-neighbor spatiotemporal diffusion coefficient at lag-1, spatial variance, spatial skewness, spatial kurtosis, and near-neighbor spatial correlation. All SEWSs show recognizable trends before the disease occurs for both noise levels $Q = 0.01$ [see Figs. 6(a)–6(f)] and $Q = 0.10$ [see Figs. 6(g)–6(l). The results indicate that these indicators can effectively identify critical transitions before the disease occurs. Moreover, these indicators have universality for different noise levels $Q$.

In Figs. 6(a) and 6(g), we present the dependence of the transient-state ensemble average $\langle\bar{\phi}\rangle$ on the growth rate $r$ for different two noise levels $Q$. For the critical region, there are increases abruptly in $\langle\bar{\phi}\rangle$; for outside the critical region, it increases smoothly with $r$. The results show that the increase of the noise level displaces the critical point toward lower values of the growth rate $r$. In addition, for the critical region, the slope of $\langle\bar{\phi}\rangle$ becomes smoother when the noise level $Q$ increases. These results suggest that the shift is gradual in the case of high heterogeneity ($Q > 0$); however, when heterogeneity is low, i.e., homogeneity ($Q = 0$), the shift is abrupt.

Figures 6(b) and 6(h) display the results of spatiotemporal diffusion coefficient at lag-1 for different noise levels $Q$. It reaches a peak (gray region). These results indicate that the spatiotemporal diffusion coefficients inside the critical region are larger than those outside. Its trend is similar to trends of spatial variance $\sigma^2$ and near-neighbor spatial correlation $\mathbb{C}(1)$ in recent work [21], which are presented below. The results verified that the near-neighbor spatiotemporal diffusion coefficient appears as a robust indicator compared with the near-neighbor spatial correlation. Hence, these findings imply that the near-neighbor spatiotemporal diffusion coefficient at lag-1 is an excellent indicator to detect the upcoming critical transition.

The spatial variance, in Figs. 6(c) and 6(i), shows a rise and a fall around the gray region. Namely, there exists a peak. For the outside this range, the spatial variance shows a straight line without slope. These results suggest that a peak is a critical threshold from health to disease state.

In Figs. 6(d) and 6(j), the spatial skewness increases first, then decreases, and finally increases with growth rate $r$. Before the gray region, spatial skewness is positive and rises with growth rate $r$ when it is close to the critical region. For the gray region, the skewness decreases and its sign becomes negative. After the gray region, the skewness gradually increases until it is close to zero. These results show that when the spatial skewness is equal to 0, it is a normal distribution and a critical threshold for upcoming critical transitions.

Figures 6(e) and 6(k) show the results of spatial kurtosis for different noise levels $Q$. The spatial kurtosis shows two

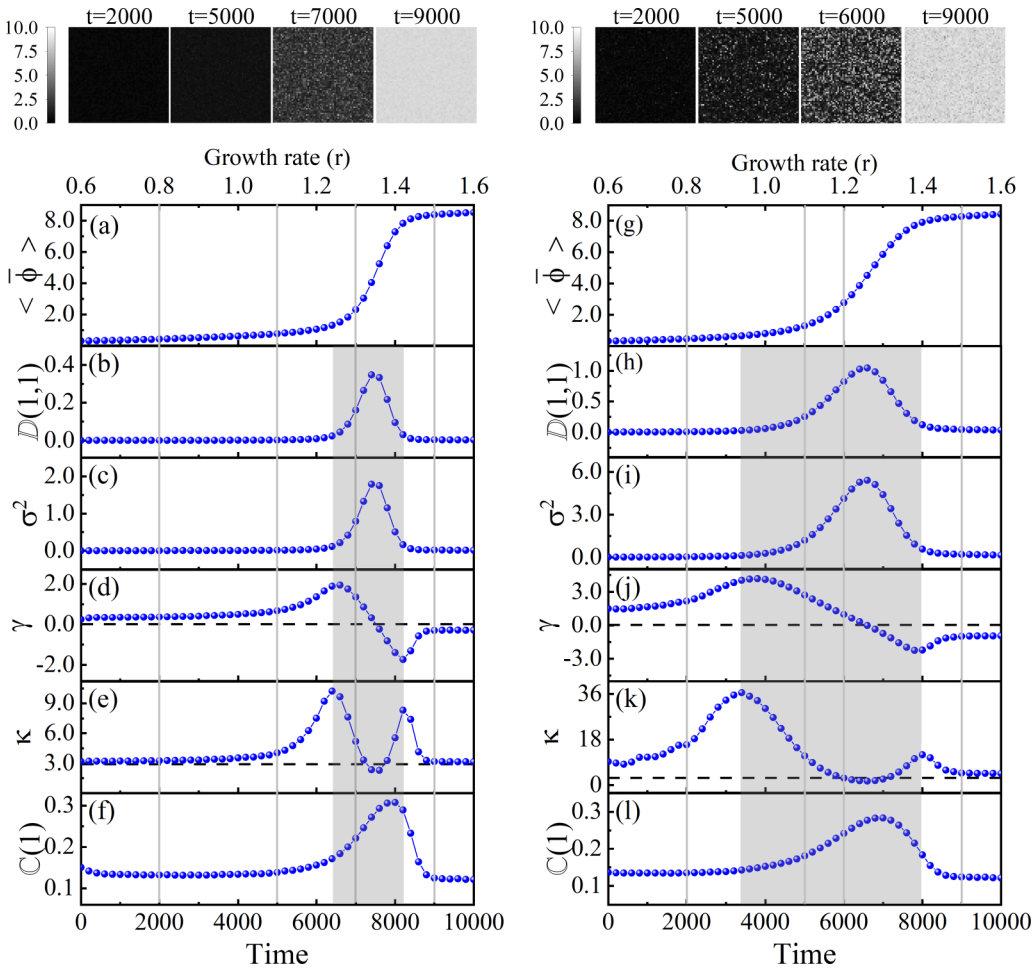


FIG. 6. [(a), (g)] The transient-state ensemble average of tumor nuclei density as a function of growth rate $r$ and simulation time. The vertical gray lines correspond to the increasing growth rate ($r$) over simulation time, where spatial snapshots are shown at the top. The snapshots are drawn in grayscale, where brighter regions represent higher tumor nucleus density. The snapshots show deviations from the ensemble average of tumor nuclei density in the snapshot, as variation in tumor nuclei density was much larger between snapshots than within. [(b)–(f), (h)–(l)] SEWSs for simulated spatial snapshots data obtained from the stochastic model of Eq. (5). Near-neighbor spatiotemporal diffusion coefficient at lag-1 [(b), (h)], spatial variance [(c), (i)], spatial skewness [(d), (j)], spatial kurtosis [(e), (k)], and near-neighbor spatial correlation [(f), (l)] as functions of growth rate $r$ and simulation time. The parameter values are $\beta = 2.0$, $K = 10.0$, $D = 0.1$, and either $Q = 0.01$ [(a)–(f)] or $Q = 0.10$ [(g)–(l)].

peaks where one locates before the critical point and the other locates after it. The corresponding values are greater than 3, indicating that as the system nears and exits the critical region, the distribution of tumor nuclei density is steeper than the normal distribution that spatial kurtosis is 3 (black dotted line). Namely, the distribution of $\kappa > 3$ is leptokurtic. Interestingly, for the critical point, the spatial kurtosis is less than 3. That is, its distribution is platykurtic. These results indicate that spatial kurtosis reached a low point in the critical threshold.

The spatial correlations in Figs. 6(f) and 6(l) display the degree of spatial correlation between neighboring patches for different noise levels $Q$. The gray region shows that spatial correlation increases with increasing growth rate $r$ until maximum spatial correlation is reached and then spatial correlation decreases with increasing growth rate $r$. Moreover, it shows a smooth straight line outside the critical region. These results suggest that spatial correlation peaks in the critical threshold.

All these results demonstrate that SEWSs show recognizable trends in spatially extended tumor-immune systems with stochasticity. These results are consistent with previous studies on spatial variance [6,40], spatial skewness [21,40], spatial kurtosis [66], and spatial correlation [20,67,68]. More importantly, the rising spatiotemporal diffusion coefficient may be an effective novel indicator of biological systems. Therefore the spatiotemporal diffusion coefficient indicator will provide a novel approach to predict the critical transition for pathology and computed tomography images [76,77].

Figure 7 shows the effect of changing the diffusion coefficient $D$ on the transient-state ensemble average $\langle\bar{\phi}\rangle$ and the following warning indicators: $\mathbb{D}(1,1)$, $\sigma^2$, $\gamma$, $\kappa$, and $\mathbb{C}(1)$. Figure 7(a) shows the transient-state ensemble average $\langle\bar{\phi}\rangle$ as a function of the growth rate $r$ for different diffusion coefficients $D$. For the critical region (gray region), the slope of $\langle\bar{\phi}\rangle$ becomes steeper when the diffusion coefficient $D$ increases. These results suggest that the shift in the case of low connectivity ($D = 0$) is gradual, as each cell shifts almost independently from its neighbor; however, it is abrupt when connectivity is high ($D > 0$).

When the diffusion coefficient $D$ increases, the value of the warning indicators decreases significantly, especially in

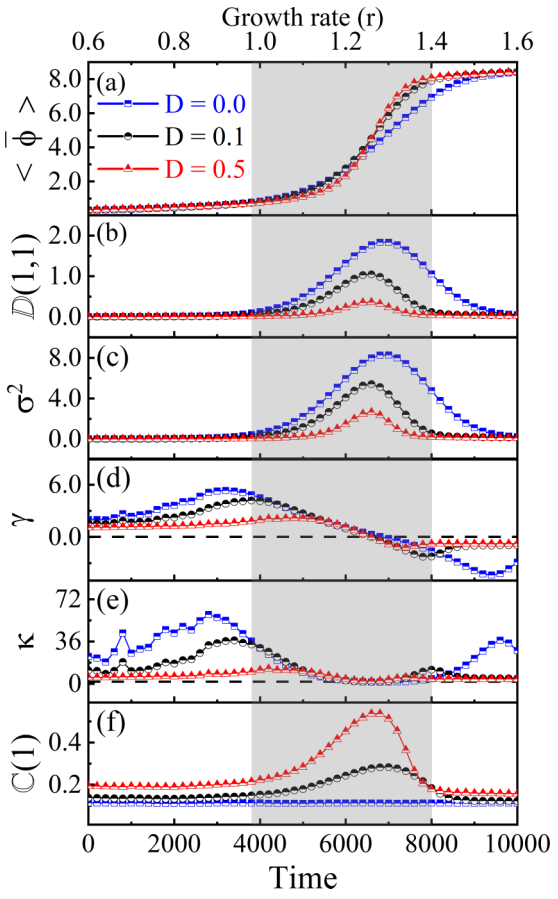


FIG. 7. (a) The transient-state ensemble average of tumor nuclei density as a function of growth rate $r$ and simulation time for different diffusion coefficients $D$. [(b)–(f)] SEWSs for simulated spatial snapshots data obtained from the stochastic model of Eq. (5). Near-neighbor spatiotemporal diffusion coefficient at lag-1 (b), spatial variance (c), spatial skewness (d), spatial kurtosis (e), and near-neighbor spatial correlation (f) as functions of growth rate $r$ and simulation time. The parameter values are $\beta = 2.0$, $K = 10.0$, and $Q = 0.1$.

the critical region [see Figs. 7(b)–7(e)]. However, as shown in Fig. 7(f), this is exactly the opposite of what is observed in Fig. 7(b). In addition, the near-neighbor spatial correlation indicator failed to predict an upcoming regime shift when connectivity was low ($D = 0$). This finding suggests that the near-neighbor spatiotemporal diffusion coefficient indicator has stronger applicability than the near-neighbor spatial correlation indicator.

Heterogeneity and a low level of connectivity may cause the system to change gradually in response to environmental change. This is because systems with different components (heterogeneity) and low connectivity lead to modularity with adaptive capacity. By contrast, homogeneity and a highly connected system may provide resistance to change until a threshold for a systemic critical transition is reached [49]. In other words, homogeneity and a high level of connectivity may cause the system to change abruptly in response to environmental change. Meanwhile, it implies that prediction of critical transition is more successful for homogeneity and a highly connected system than for heterogeneity and a low-level connected system. These findings are similar to those reported in the literature [20,49].

## IV. DISCUSSION

In this paper, we study the spatial tumor-immune system with stochasticity via theoretical analysis and numerical simulations to anticipate critical transitions from health to disease state. Using the Langevin equation, the Fokker-Planck equation, and the MFA assumption, the stationary probability distribution solutions are derived theoretically. To verify theoretical results, we also present corresponding numerical results. It is shown that the numerical results agree well with the theoretical prediction for a small noise level, suggesting that our results are credible. Based on the theoretical analysis and numerical simulation, we investigate how noise levels $Q$ and growth rates $r$ affect the spatial tumor-immune system with stochasticity. Our results suggest that when there is a bistable state in the system, the health state becomes more and more stable than the disease state as the noise increases. Moreover, the system goes from a low tumor nuclei density state (health) to a high tumor nuclei density state (disease) through a bistable region as the growth rate $r$ increases. We not only certify the findings of previous works [60,78] but also exploit SEWSs to predict upcoming critical transitions, which have been extensively studied in ecosystems [20,21,40]. Here we focus on a spatiotemporal diffusion coefficient that combines the spatial snapshots with the temporal dynamics, providing new and reliable SEWSs for the impending critical transitions in the spatial tumor-immune system. The critical transition from health to disease is easily captured in the plot of spatial averages in Figs. 6(a) and 6(g) and the spatial indicators in Figs. 6(b)–6(f) and 6(h)–6(l), which show substantial changes during the transition period. The spatial averages are increasing slightly with simulation time up to 7000 ($r = 1.3$) and 6000 ($r = 1.2$), as shown in Figs. 6(a) and 6(g). There are rising trends of the near-neighbor spatiotemporal diffusion coefficient, the spatial variance, and the near-neighbor spatial correlation when the system closes to critical transitions. The spatial skewness shows a sharp variety from a positive to a negative value in the critical region, revealing the system traversing in this region and approaching the disease state. The spatial kurtosis of tumor nuclei density changes from leptokurtic to platykurtic and leptokurtic again in this region and immediately later. When the spatial average does not display a clear disease state, the near-neighbor spatiotemporal diffusion coefficient, spatial variance, spatial skewness, spatial kurtosis, and near-neighbor spatial correlation provide us five potential early warning signals of an impending transition. Hence these indicators can effectively identify critical transitions before the disease occurs.

The TME is heterogeneous and fluctuating. Therefore a significant challenge for modeling the TME is to analyze spatiotemporal fluctuations in complex environments. It is important to develop models of tumor growth that include a representation of an immune response. In the future, we hope to precisely consider the effect of tumor-immune cell interactions [79,80]. Although our work is insufficient to accurately describe the real tumor evolution, it provides a way to analyze spatially extended tumor-immune systems with stochasticity.

We expect that these findings will stimulate theoretical and experimental work to provide practical SEWSs for the prevention of cancer.

With the advancement of technology, the increasing availability and resolution of pathology images data [76,81] provide an opportunity to detect impending critical transitions. Previous studies have connected the distance from the brightest voxel in $^{18}$F-FDG PET imaging of breast and lung cancer patients to the tumor centroid with the evolutionary dynamics of tumor growth [77]. This work is similar to our study where spatially correlated features are extracted from spatial snapshots to predict SEWSs. In the future, we hope that these findings will stimulate machine-learning techniques to provide a valuable way for the earlier clinical diagnosis of cancer. All indicators of SEWSs are also applicable to remotely sensed imagery of ecosystems [82,83]. Our results reveal that anticipating critical transitions is imperative to prevent the onset and progression of cancer, which may intercept abrupt shifts from health to disease state.

## ACKNOWLEDGMENTS

This work was supported by the Yunnan Fundamental Research Projects (Grants No. 2019FI002, No. 202101AS070018, and No. 202101AV070015), the Yunnan Ten Thousand Talents Plan Young & Elite Talents Project, the Yunnan Province Computational Physics and Applied Science and Technology Innovation Team, and the National Natural Science Foundation of China under Grants No. 12175193 and No. 11775186.

## APPENDIX A: DISCRETE POPULATION MODEL OF TUMOR GROWTH

The discrete tumor growth model by adding the immune item $p(\phi_t) = \beta\phi_t^2/(1+\phi_t^2)$ is

$$\phi_{t+1} = r\phi_t\left(1-\frac{\phi_t}{K}\right) - \frac{\beta\phi_t^2}{1+\phi_t^2}, \tag{A1}$$

where $\phi_t$ represents the initial tumor nuclei density, $\phi_{t+1}$ is the density after a single interval of time step, $r$ denotes the growth rate of the tumor cells, $K$ stand for carrying capacity and $\beta$ indicates immune coefficient. The result is shown in Fig. 1. The negative (positive) values of the Lyapunov exponent ($\lambda$) indicate that the dynamics of system are periodical (chaotic). Moreover, the Lyapunov exponent of $\lambda = 0$ represents the bifurcation point.

## APPENDIX B: STOCHASTIC ALGORITHM

The SPDE the generic form given by

$$\frac{\partial\phi(\mathbf{x},t)}{\partial t} = f[\phi(\mathbf{x},t)] + D\nabla^2\phi(\mathbf{x},t) - g[\phi(\mathbf{x},t)]\eta(\mathbf{x},t). \tag{B1}$$

The Laplacian operator of Eq. (B1) in a lattice form can be discretized as [38,39,59,84]

$$D\nabla^2\phi(\mathbf{x},t) = \sum_j \nabla_{ij}^2\phi_j(t) \equiv \frac{D}{2d\,\Delta x^d}\sum_{j\in nn(i)}(\phi_j-\phi_i), \tag{B2}$$

where $nn(i)$ is the set of the $2d$ nearest neighbors of site $i$. Let $h[\phi_i(t)] = D/(2d\,\Delta x^d)\sum_{j\in nn(i)}[\phi_j(t)-\phi_i(t)]$. We wished to write the SPDE in a discrete space as follows:

$$\frac{\mathrm{d}\phi_i(t)}{\mathrm{d}t} = f[\phi_i(t)] + h[\phi_i(t)] - g[\phi_i(t)]\eta_i(t). \tag{B3}$$

After the formal integration of Eq. (B3) in an interval of very short time $(t, t+\Delta t)$, we obtain

$$\phi_i(t+\Delta t) = \phi_i(t) + \int_t^{t+\Delta t} f[\phi_i(t')]\,dt' + \int_t^{t+\Delta t} h[\phi_i(t')]dt' - \int_t^{t+\Delta t} g[\phi_i(t')]\eta_i(t')\,dt'. \tag{B4}$$

The first and second integral terms in Eq. (B4) are performed via the second-order predictor-corrector algorithm; the third integral term in Eq. (B4) is implemented by the standard Heun algorithm, and we make the following assumptions, respectively,

$$\int_t^{t+\Delta t} f[\phi_i(t')]\,dt' = \left(\frac{f[\phi_i(t)]+f[\tilde{\phi}_i(t)]}{2}\right)\Delta t, \tag{B5}$$

$$\int_t^{t+\Delta t} h[\phi_i(t')]\,dt' = \left(\frac{h[\phi_i(t)]+h[\tilde{\phi}_i(t)]}{2}\right)\Delta t, \tag{B6}$$

$$\int_t^{t+\Delta t} g[\phi_i(t')]\eta_i(t')\,dt' = \left(\frac{g[\phi_i(t)]+g[\tilde{\phi}_i(t)]}{2}\right)\mathcal{X}_i(t), \tag{B7}$$

where the predictor step is the first-order algorithm for the Itô interpretation ($\alpha = 0$),

$$\tilde{\phi}_i(t) = \phi_i(t) + f[\phi_i(t)]\Delta t + h[\phi_i(t)]\Delta t - g[\phi_i(t)]\mathcal{X}_i(t), \tag{B8}$$

and the corrector step uses the Stratonovich interpretation ($\alpha = 1/2$),

$$\phi_i(t+\Delta t) = \phi_i(t) + \left(\frac{f[\phi_i(t)]+f[\tilde{\phi}_i(t)]}{2}\right)\Delta t + \left(\frac{h[\phi_i(t)]+h[\tilde{\phi}_i(t)]}{2}\right)\Delta t - \{(1-\alpha)g[\phi_i(t)] + \alpha g[\tilde{\phi}_i(t)]\}\mathcal{X}_i(t). \tag{B9}$$

Therefore the discrete-spatiotemporal stochastic algorithm of the Heun′s predictor-corrector is as follows:

$$\phi_i(t+\Delta t) = \phi_i(t) + \left(\frac{f[\phi_i(t)]+f[\tilde{\phi}_i(t)]}{2}\right)\Delta t + \left(\frac{h[\phi_i(t)]+h[\tilde{\phi}_i(t)]}{2}\right)\Delta t - \left(\frac{g[\phi_i(t)]+g[\tilde{\phi}_i(t)]}{2}\right)\mathcal{X}_i(t), \tag{B10}$$

where

$$\mathcal{X}_i(t) = \sqrt{\frac{2Q\Delta t}{\Delta x^d}}\gamma_i. \tag{B11}$$

Here $\gamma_i$ are independent Gaussian random numbers with zero mean and variance equal to 1 and using Box-Muller-Wiener algorithm to implement them.

[1] C. Trefois, P. M. Antony, J. Goncalves, A. Skupin, and R. Balling, Critical transitions in chronic disease: Transferring concepts from ecology to systems medicine, Curr. Opin. Biotechnol. **34**, 48 (2015).

[2] M. Scheffer, J. Bascompte, W. A. Brock, V. Brovkin, S. R. Carpenter, V. Dakos, H. Held, E. H. van Nes, M. Rietkerk, and G. Sugihara, Early-warning signals for critical transitions, Nature (London) **461**, 53 (2009).

[3] M. Scheffer, *Critical Transitions in Nature and Society* (Princeton University Press, Princeton, 2009), Vol. 16.

[4] M. Scheffer, S. Carpenter, J. A. Foley, C. Folke, and B. Walker, Catastrophic shifts in ecosystems, Nature (London) **413**, 591 (2001).

[5] S. R. Carpenter, Eutrophication of aquatic ecosystems: Bistability and soil phosphorus, Proc. Natl. Acad. Sci. USA **102**, 10002 (2005).

[6] S. R. Carpenter and W. A. Brock, Rising variance: A leading indicator of ecological transition, Ecol. Lett. **9**, 311 (2006).

[7] R. Wang, J. A. Dearing, P. G. Langdon, E. Zhang, X. Yang, V. Dakos, and M. Scheffer, Flickering gives early warning signals of a critical transition to a eutrophic lake state, Nature (London) **492**, 419 (2012).

[8] S. R. Carpenter, J. J. Cole, M. L. Pace, R. Batt, W. Brock, T. Cline, J. Coloso, J. R. Hodgson, J. F. Kitchell, D. A. Seekell *et al.*, Early warnings of regime shifts: A whole-ecosystem experiment, Science **332**, 1079 (2011).

[9] P. J. Mumby, A. Hastings, and H. J. Edwards, Thresholds and the resilience of caribbean coral reefs, Nature (London) **450**, 98 (2007).

[10] T. P. Hughes, N. A. Graham, J. B. Jackson, P. J. Mumby, and R. S. Steneck, Rising to the challenge of sustaining coral reef resilience, Trends Ecol. Evol. **25**, 633 (2010).

[11] N. Boers, Early-warning signals for dansgaard-oeschger events in a high-resolution ice core record, Nat. Commun. **9**, 2556 (2018).

[12] L. Lahti, J. Salojärvi, A. Salonen, M. Scheffer, and W. M. De Vos, Tipping elements in the human intestinal ecosystem, Nat. Commun. **5**, 4344 (2014).

[13] I. A. van de Leemput, M. Wichers, A. O. Cramer, D. Borsboom, F. Tuerlinckx, P. Kuppens, E. H. van Nes, W. Viechtbauer, E. J. Giltay, S. H. Aggen *et al.*, Critical slowing down as early warning for the onset and termination of depression, Proc. Natl. Acad. Sci. USA **111**, 87 (2014).

[14] P. E. McSharry, L. A. Smith, and L. Tarassenko, Prediction of epileptic seizures: Are nonlinear methods relevant? Nat. Med. **9**, 241 (2003).

[15] M. A. Kramer, W. Truccolo, U. T. Eden, K. Q. Lepage, L. R. Hochberg, E. N. Eskandar, J. R. Madsen, J. W. Lee, A. Maheshwari, E. Halgren *et al.*, Human seizures self-terminate across spatial scales via a critical transition, Proc. Natl. Acad. Sci. USA **109**, 21116 (2012).

[16] A. Kianercy, R. Veltri, and K. J. Pienta, Critical transitions in a game theoretic model of tumour metabolism, Interface Focus **4**, 20140014 (2014).

[17] M. Rietkerk, M. C. Boerlijst, F. van Langevelde, R. HilleRisLambers, J. V. de Koppel, L. Kumar, H. H. Prins, and A. de Roos, Self-organization of vegetation in arid ecosystems, Am. Nat. **160**, 524 (2002).

[18] N. Shnerb, P. Sarah, H. Lavee, and S. Solomon, Reactive Glass and Vegetation Patterns, Phys. Rev. Lett. **90**, 038101 (2003).

[19] S. Kéfi, M. Rietkerk, M. van Baalen, and M. Loreau, Local facilitation, bistability and transitions in arid ecosystems, Theor. Popul. Biol. **71**, 367 (2007).

[20] V. Dakos, E. H. van Nes, R. Donangelo, H. Fort, and M. Scheffer, Spatial correlation as leading indicator of catastrophic shifts, Theor. Ecol. **3**, 163 (2010).

[21] S. Kefi, V. Guttal, W. A. Brock, S. R. Carpenter, A. M. Ellison, V. N. Livina, D. A. Seekell, M. Scheffer, E. H. van Nes, and V. Dakos, Early warning signals of ecological transitions: methods for spatial patterns, PLoS One **9**, e92097 (2014).

[22] P. C. Hohenberg and B. I. Halperin, Theory of dynamic critical phenomena, Rev. Mod. Phys. **49**, 435 (1977).

[23] J. Swift and P. C. Hohenberg, Hydrodynamic fluctuations at the convective instability, Phys. Rev. A **15**, 319 (1977).

[24] M. C. Cross and P. C. Hohenberg, Pattern formation outside of equilibrium, Rev. Mod. Phys. **65**, 851 (1993).

[25] J. J. Tyson and P. C. Fife, Target patterns in a realistic model of the belousov–zhabotinskii reaction, J. Chem. Phys. **73**, 2224 (1980).

[26] D. Barkley, A model for fast computer simulation of waves in excitable media, Physica D **49**, 61 (1991).

[27] A. Pikovsky, J. Kurths, M. Rosenblum, and J. Kurths, *Synchronization: A Universal Concept in Nonlinear Sciences* (Cambridge University Press, Cambridge, 2002), No. 12.

[28] H. Hong, H. Park, and M. Choi, Collective synchronization in spatially extended systems of coupled oscillators with random frequencies, Phys. Rev. E **72**, 036217 (2005).

[29] M. A. Chaplain, M. Ganesh, and I. G. Graham, Spatio-temporal pattern formation on spherical surfaces: Numerical simulation and application to solid tumour growth, J. Math. Biol. **42**, 387 (2001).

[30] P. Macklin and J. Lowengrub, Nonlinear simulation of the effect of microenvironment on tumor growth, J. Theor. Biol. **245**, 677 (2007).

[31] S. C. Ferreira, M. Martins, and M. Vilela, Reaction-diffusion model for the growth of avascular tumor, Phys. Rev. E **65**, 021907 (2002).

[32] M. Martin and T. Risler, Viscocapillary instability in cellular spheroids, New J. Phys. **23**, 033032 (2021).

[33] E. Khain and L. M. Sander, Dynamics and Pattern Formation in Invasive Tumor Growth, Phys. Rev. Lett. **96**, 188103 (2006).

[34] T. Risler and M. Basan, Morphological instabilities of stratified epithelia: A mechanical instability in tumour formation, New J. Phys. **15**, 065011 (2013).

[35] B. Ai, X. Wang, G. Liu, and L. Liu, Correlated noise in a logistic growth model, Phys. Rev. E **67**, 022903 (2003).

[36] C. Zeng and H. Wang, Colored noise enhanced stability in a tumor cell growth system under immune response, J. Stat. Phys. **141**, 889 (2010).

[37] A. d'Onofrio, Bounded-noise-induced transitions in a tumor-immune system interplay, Phys. Rev. E **81**, 021923 (2010).

[38] F. Sagués, J. M. Sancho, and J. García-Ojalvo, Spatiotemporal order out of noise, Rev. Mod. Phys. **79**, 829 (2007).

[39] C. Van den Broeck, J. Parrondo, and R. Toral, Noise-induced nonequilibrium phase transition, Phys. Rev. Lett. **73**, 3395 (1994).

[40] V. Guttal and C. Jayaprakash, Spatial variance and spatial skewness: Leading indicators of regime shifts in spatial ecological systems, Theor. Ecol. **2**, 3 (2009).

[41] S. Qin and C. Tang, Early-warning signals of critical transition: Effect of extrinsic noise, Phys. Rev. E **97**, 032406 (2018).

[42] M. Scheffer and S. R. Carpenter, Catastrophic regime shifts in ecosystems: linking theory to observation, Trends Ecol. Evol. **18**, 648 (2003).

[43] M. Hirota, M. Holmgren, E. H. van Nes, and M. Scheffer, Global resilience of tropical forest and savanna to critical transitions, Science **334**, 232 (2011).

[44] T. M. Lenton, H. Held, E. Kriegler, J. W. Hall, W. Lucht, S. Rahmstorf, and H. J. Schellnhuber, Tipping elements in the earth's climate system, Proc. Natl. Acad. Sci. USA **105**, 1786 (2008).

[45] P. Milanowski and P. Suffczynski, Seizures start without common signatures of critical transition, Int. J. Neur. Syst. **26**, 1650053 (2016).

[46] A. Ghadami, E. Gourgou, and B. I. Epureanu, Rate of recovery from perturbations as a means to forecast future stability of living systems, Sci. Rep. **8**, 9271 (2018).

[47] R. M. May, S. A. Levin, and G. Sugihara, Ecology for bankers, Nature (London) **451**, 893 (2008).

[48] P. Wang, L. Zong, and Y. Ma, An integrated early warning system for stock market turbulence, Expert Syst. Appl. **153**, 113463 (2020).

[49] M. Scheffer, S. R. Carpenter, T. M. Lenton, J. Bascompte, W. Brock, V. Dakos, J. van de Koppel, I. A. van de Leemput, S. A. Levin, E. H. van Nes *et al.*, Anticipating critical transitions, Science **338**, 344 (2012).

[50] D. Ludwig, D. D. Jones, and C. S. Holling, Qualitative analysis of insect outbreak systems: The spruce budworm and forest, J. Anim. Ecol. **47**, 315 (1978).

[51] J. B. Swann, M. J. Smyth *et al.*, Immune surveillance of tumors, J. Clin. Invest. **117**, 1137 (2007).

[52] I. Noy-Meir, Stability of grazing systems: An application of predator-prey graphs, The Journal of Ecology **63**, 459 (1975).

[53] R. M. May, Thresholds and breakpoints in ecosystems with a multiplicity of stable states, Nature (London) **269**, 471 (1977).

[54] J. D. Murray, *Mathematical Biology: I. An Introduction* (Springer Science & Business Media, Berlin, 2007), Vol. 17.

[55] S. H. Strogatz, *Nonlinear Dynamics and Chaos with Student Solutions Manual: With Applications to Physics, Biology, Chemistry, and Engineering* (CRC Press, Boca Raton, 2015).

[56] S. S. Cross and D. W. Cotton, Chaos and antichaos in pathology, Hum. Pathol. **25**, 630 (1994).

[57] A. Huebner, M. Dietzen, and N. McGranahan, Snapshot: Tumor evolution, Cell **184**, 1650 (2021).

[58] J. Li, System with temporal-spatial noise, Phys. Rev. E **67**, 061108 (2003).

[59] O. Carrillo, M. Ibañes, J. García-Ojalvo, J. Casademunt, and J. Sancho, Intrinsic noise-induced phase transitions: Beyond the noise interpretation, Phys. Rev. E **67**, 046110 (2003).

[60] W. Zhong, Y. Shao, and Z. He, Spatiotemporal fluctuation-induced transition in a tumor model with immune surveillance, Phys. Rev. E **74**, 011916 (2006).

[61] H. Risken, Fokker-planck equation, In *The Fokker-Planck Equation* (Springer-Verlag, Berlin, 1996), pp. 63–95.

[62] D. Wu and S. Zhu, Effects of cross-correlated noises on the transport of active brownian particles, Phys. Rev. E **90**, 012131 (2014).

[63] A. W. Lau and T. C. Lubensky, State-dependent diffusion: Thermodynamic consistency and its path integral formulation, Phys. Rev. E **76**, 011123 (2007).

[64] D. Mei, C. Xie, and L. Zhang, The stationary properties and the state transition of the tumor cell growth mode, Eur. Phys. J. B **41**, 107 (2004).

[65] W. Zhong, Y. Shao, and Z. He, Pure multiplicative stochastic resonance of a theoretical anti-tumor model with seasonal modulability, Phys. Rev. E **73**, 060902(R) (2006).

[66] S. Orozco-Fuentes, G. Griffiths, M. Holmes, R. Ettelaie, J. Smith, A. Baggaley, and N. Parker, Early warning signals in plant disease outbreaks, Ecol. Modell. **393**, 12 (2019).

[67] J. M. Drake and B. D. Griffen, Early warning signals of extinction in deteriorating environments, Nature (London) **467**, 456 (2010).

[68] C. Meisel and C. Kuehn, Scaling effects and spatio-temporal multilevel dynamics in epileptic seizures, PLoS One **7**, e30371 (2012).

[69] B. Lindner and E. M. Nicola, Critical Asymmetry for Giant Diffusion of Active Brownian Particles, Phys. Rev. Lett. **101**, 190603 (2008).

[70] J. Spiechowicz, P. Hänggi, and J. Łuczka, Coexistence of absolute negative mobility and anomalous diffusion, New J. Phys. **21**, 083029 (2019).

[71] K. Białas, J. Łuczka, P. Hänggi, and J. Spiechowicz, Colossal brownian yet non-gaussian diffusion induced by nonequilibrium noise, Phys. Rev. E **102**, 042121 (2020).

[72] Y. Luo, C. Zeng, and B. Ai, Strong-chaos-caused negative mobility in a periodic substrate potential, Phys. Rev. E **102**, 042114 (2020).

[73] D. J. Higham, An algorithmic introduction to numerical simulation of stochastic differential equations, SIAM Rev. **43**, 525 (2001).

[74] V. Dakos, S. R. Carpenter, T. Cline, and L. Lahti, Early Warning Signals Toolbox for Detecting Critical Transitions in Time-series, http://www.early-warning-signals.org (2013).

[75] V. Dakos, S. R. Carpenter, W. A. Brock, A. M. Ellison, V. Guttal, A. R. Ives, S. Kéfi, V. Livina, D. A. Seekell, E. H. van Nes *et al.*, Methods for detecting early warnings of critical transitions in time series illustrated using simulated ecological data, PLoS One **7**, e41010 (2012).

[76] S. Wang, R. Rong, D. M. Yang, J. Fujimoto, S. Yan, L. Cai, L. Yang, D. Luo, C. Behrens, E. R. Parra *et al.*, Computational staining of pathology images to study the tumor microenvironment in lung cancer, Cancer Res. **80**, 2056 (2020).

[77] J. Jiménez-Sánchez, J. J. Bosque, G. A. J. Londoño, D. Molina-García, Á. Martínez, J. Pérez-Beteta, C. Ortega-Sabater, A. F. H. Martínez, A. M. G. Vicente, G. F. Calvo *et al.*, Evolutionary dynamics at the tumor edge reveal metabolic imaging biomarkers, Proc. Natl. Acad. Sci. USA **118**, e2018110118 (2021).

[78] W. Zhong, Y. Shao, L. Li, F. Wang, and Z. He, Spatiotemporal noise triggering infiltrative tumor growth with immunosurveillance, Europhys. Lett. **82**, 20003 (2008).

[79] V. A. Kuznetsov, I. A. Makalkin, M. A. Taylor, and A. S. Perelson, Nonlinear dynamics of immunogenic tumors: Param-

eter estimation and global bifurcation analysis, Bull. Math. Biol. **56**, 295 (1994).

[80] L. G. de Pillis, A. E. Radunskaya, and C. L. Wiseman, A validated mathematical model of cell-mediated immune response to tumor growth, Cancer Res. **65**, 7950 (2005).

[81] J. K. Chan, The wonderful colors of the hematoxylin–eosin stain in diagnostic surgical pathology, Int. J. Surg. Pathol. **22**, 12 (2014).

[82] B. M. Rogers, K. Solvik, E. H. Hogg, J. Ju, J. G. Masek, M. Michaelian, L. T. Berner, and S. J. Goetz, Detecting early warning signals of tree mortality in boreal north america using multiscale satellite data, Glob Change Biol **24**, 2284 (2018).

[83] J. J. Nijp, A. J. Temme, G. A. van Voorn, L. Kooistra, G. M. Hengeveld, M. B. Soons, A. J. Teuling, and J. Wallinga, Spatial early warning signals for impending regime shifts: A practical framework for application in real-world landscapes, Glob Change Biol **25**, 1905 (2019).

[84] C. Van den Broeck, J. Parrondo, R. Toral, and R. Kawai, Nonequilibrium phase transitions induced by multiplicative noise, Phys. Rev. E **55**, 4084 (1997).